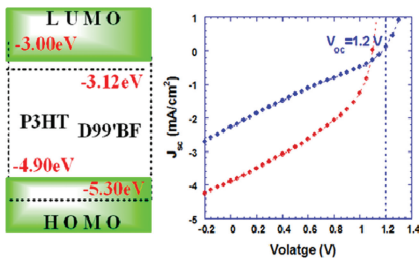


COMMUNICATIONS

Solar Cells

X. Gong, M. Tong, F. G. Brunetti,
J. Seo, Y. Sun, D. Moses, F. Wudl,*
A. J. heeger*x-xx

**Bulk Heterojunction Solar Cells with
Large Open-Circuit Voltage: Electron
Transfer with Small Donor-Acceptor
Energy Offset**



Photoinduced electron transfer is observed in polymer bulk heterojunction solar cells with very small interfacial energy offset. The results imply that open circuit voltage values close to the band gap of the semiconducting polymer should be possible for polymer bulk heterojunction solar cells just as for inorganic solar cells.

Bulk Heterojunction Solar Cells with Large Open-Circuit Voltage: Electron Transfer with Small Donor-Acceptor Energy Offset

Xiong Gong, Minghong Tong, Fulvio G. Brunetti, Junghwa Seo, Yanming Sun, Daniel Moses, Fred Wudl,* and Alan J. Heeger*

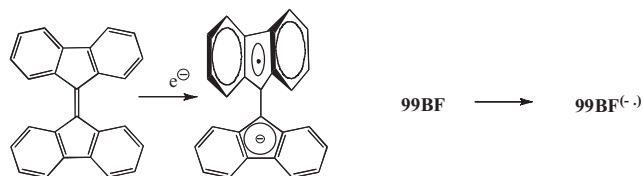
Power conversion efficiencies (PCEs) (in response to solar AM1.5 radiation) as high as 6–8% have been reported for bulk heterojunction (BHJ) polymer solar cells.^[1,2] In order to attain PCEs over 10%, BHJ materials capable of generating larger open circuit voltage (V_{oc}) are required.^[3,4] One approach to increase V_{oc} is to develop low-bandgap semiconducting polymers with deeper highest occupied molecular orbital (HOMO) energies. An alternative approach is to develop new electron acceptors with higher lowest unoccupied molecular orbital (LUMO) energies. The pathway to low-bandgap semiconducting polymers with deeper HOMOs is well understood, and BHJ solar cells fabricated by semiconducting polymers with deeper HOMOs have successfully exhibited larger V_{oc} .^[5] However, the discovery of new (non-fullerene) electron acceptors with higher LUMOs remains undeveloped.^[6]

In all BHJ materials studied to date, a significant fraction of the photon energy (typically more than half) is given up in the charge transfer process because of the large energy offset between the LUMO of the donor polymer and the LUMO of the acceptor molecule. The factors that limit the V_{oc} in BHJ solar cells remain controversial. The commonly accepted reason for this loss is that in order to obtain the required charge transfer, the LUMO offset must be larger than the exciton binding energy in the donor polymer. Here we demonstrate ultrafast charge transfer and the generation of photocurrent observed from BHJ PSCs even though the LUMO energy offset between the donor polymer and the acceptor molecule is only 0.12 eV. As a result, $V_{oc} = 1.20$ V. The results clarify the path toward higher PCE by demonstrating that charge transfer and charge separation can occur in polymer BHJ systems with small donor-acceptor LUMO offset. Thus, V_{oc} values close to the theoretical maximum, the band gap of the semiconducting polymer, should be possible for BHJ solar cells just as for inorganic solar cells.

Electron acceptors, by definition, are mild-to-moderate oxidizing agents. A working hypothesis is that the large asymmetry in forward to back charge transfer rates shown by polymer:fullerene systems originates from strain-relief

accompanying addition of an electron to the strained quasi- sp^2 carbon cluster. The strain-relief is a result of rehybridization from almost sp^2 to essentially sp^3 at the carbanionic carbon and to a lesser degree at the adjacent free radical site. This is a unique feature of buckminsterfullerene and its adducts such as [6,6]-phenyl- C_{61} -butyric acid methyl ester (PCBM). Many fullerene derivatives have been synthesized,^[7] yet with the exception of the C_{70} analog, PCBM continues to be the “fruit fly” of BHJ solar cell research. With fullerenes, however, one has only very moderate control of the HOMO-LUMO gap or the energy of the LUMO relative to vacuum because C_{60} can only be modified by addition reactions and not substitution reaction. As a result, in attempts to shift the electronic energy levels of a fullerene acceptor, one cannot use the concept of resonance but only inductive effects. Unfortunately inductive effects are weak and fall off exponentially with distance. Therefore it is important to investigate new approaches to electron acceptors.

Another source of strain, well-known in physical organic chemistry, is provided by steric inhibition of co-planarity of adjacent sp^2 hybridized carbon atoms by twisting. An example is the electron acceptor, 9,9'-bifluorenylidene (99BF):



With the goal of reducing the offset between the LUMO energies of donor semiconducting polymers and acceptor molecules and thereby minimizing energy loss in BHJ solar cells, we directed our attention to the development of 9,9'-bifluorenylidene derivatives, specifically to 12-(3,6-dimethoxy-fluorenylidene)-12H-dibenzo[b,h]fluorene (D99'BF), as a new π -surface electron acceptor.

The molecular structures of D99'BF and poly(3-hexylthiophene) (P3HT) are shown in Figure 1a. The molecular structure of *t*-Bu-PBD- SO_3Na (*t*-Bu-PBD: 2-*tert*-butylphenyl-5-bi-phenyl-1,3,4-oxadiazole) is also indicated in Figure 1a. The normalized UV-visible absorption of thin films of pristine P3HT, D99'BF and the P3HT:D99'BF phase separated BHJ material are shown in Figure 1b. The absorption band of pristine P3HT with onset near 2 eV and peak at 2.7 eV are known to arise from the lowest energy interband transition (across the band gap). The absorption peak at 2.39 eV for pristine D99'BF results

Dr. X. Gong, Dr. M. Tong, Dr. F.G. Brunetti, J. Seo, Y. Sun,
Dr. D. Moses, Prof. F. Wudl, Prof. A. J. Heeger
Center for Polymers and Organic Solids
University of California Santa Barbara
Santa Barbara, CA 93106, USA
E-mail: wudl@chem.ucsb.edu; ajhe@physics.ucsb.edu

DOI: 10.1002/adma.201003768

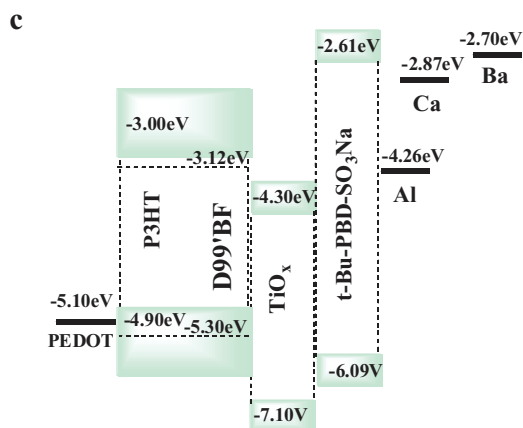
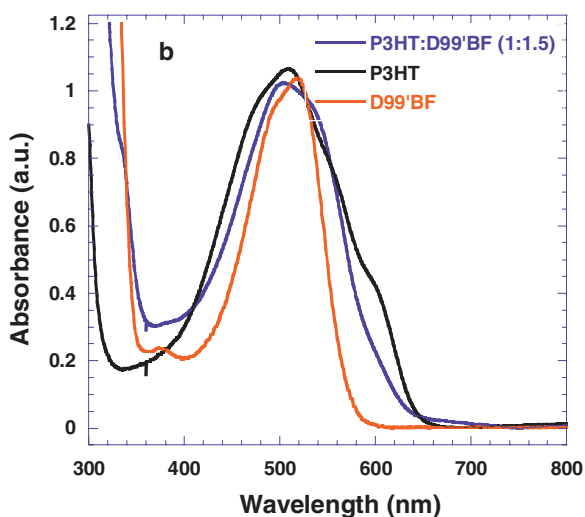
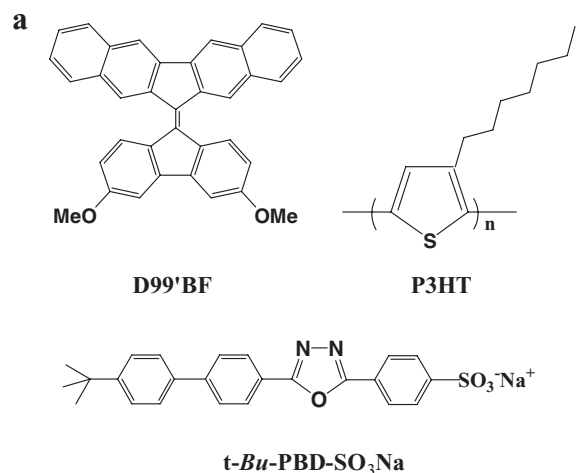


Figure 1. (a) Molecular structures of P3HT, D99'BF and t-Bu-PBD-SO₃Na; (b) Absorption spectra of pristine P3HT, D99'BF and P3HT:D99'BF, and (c) Energy level diagram showing the HOMO and LUMO energies of P3HT, D99'BF, t-Bu-PBD-SO₃Na and TiO_x, and the work functions of PEDOT:PSS, Al, Ca and Ba.

from the HOMO-LUMO transition in D99'BF. The absorption spectrum of the P3HT:D99'BF BHJ material is a superposition of the absorption features of both P3HT and D99'BF. Addition of 60% w/w of D99'BF does not significantly alter the absorption of P3HT; the additional absorption from 3.5 eV to 4 eV that appears in the spectrum of P3HT:D99'BF originates from D99'BF. The data in Figure 1b demonstrate that D99'BF adds significantly to the optical density of the BHJ material.

Figure 2 shows the ultraviolet photoelectron spectroscopy (UPS) spectra taken for P3HT and D99'BF thin films. The abscissa is the binding energy relative to the Fermi energy (E_F) of Au, which is defined by the energy of the electron before excitation relative to the vacuum level. Figure 2a shows the high binding energy cutoff (E_{cutoff}) of P3HT and D99'BF thin films; E_{cutoff} is determined by linear extrapolation to zero of the yield of secondary electrons. From Figure 2a, $E_{cutoff} = 16.7 \pm 0.03$ eV for P3HT and $E_{cutoff} = 16.5 \pm 0.03$ eV for D99'BF. Figure 2b

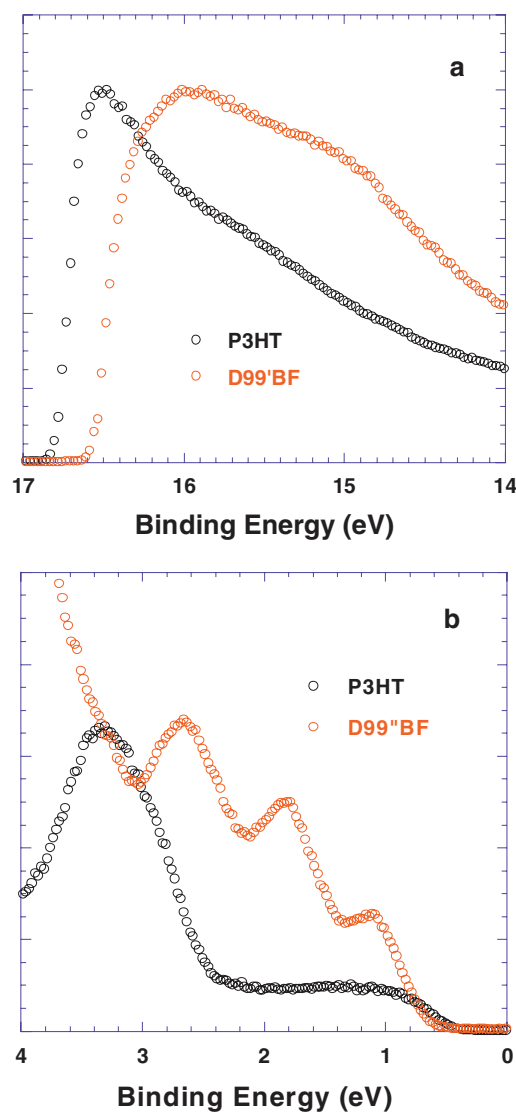


Figure 2. UPS spectra of (a) the secondary edge region and (b) the HOMO region of P3HT and D99'BF.

shows the HOMO region (0–4 eV) for P3HT and D99'BF thin films. The HOMO energies are determined using the incident photon energy, $h\nu = 21.2$ eV, E_{cutoff} , and the E_{onset} (the onset of the P3HT or D99'BF films relative to the E_{F} of Au). From the data in Figure 2b, $E_{\text{onset}} = 0.4 \pm 0.03$ eV for P3HT and $E_{\text{onset}} = 0.6 \pm 0.03$ eV for D99'BF. The HOMO energies are thus obtained directly from the UPS measurements,

For P3HT, $E_{\text{HOMO}} = 4.9 \pm 0.06$ eV; for D99'BF, $E_{\text{HOMO}} = 5.30 \pm 0.06$ eV.^[8,9] The LUMO energies were calculated using the HOMO levels and the optical gaps (E_{g}) obtained from the onset of absorption shown in Figure 1c; $E_{\text{g}} = 1.90$ eV for P3HT and $E_{\text{g}} = 2.18$ eV for D99'BF. Thus for P3HT, $E_{\text{LUMO}} = 3.00 \pm 0.06$ eV; and for D99'BF, $E_{\text{LUMO}} = 3.12 \pm 0.06$ eV for D99'BF.

The summary energy level diagram is shown in Figure 1c, with HOMO and LUMO energies for P3HT, D99'BF, *t*-Bu-PBD-SO₃Na, and TiO_x. The workfunctions of PEDOT:PSS, Al, Ba and Ca are also indicated in Figure 1c.

According to Figure 1c, photo-induced hole transfer from D99'BF to P3HT is to be expected; the HOMO-HOMO offset is 0.4 eV. One might expect, however, that photo-induced electron transfer from P3HT to D99'BF would be inefficient (or even not occur) because of the small difference between the LUMO energies of P3HT and D99'BF.^[10,11] Consequently, we have studied the photoluminescence (PL), photoconductivity (PC) and time resolved photoinduced absorption (PIA) of P3HT:D99'BF thin films and compared the results with corresponding data from pristine P3HT.

PL spectra of pristine P3HT and P3HT:D99'BF are shown in Figure 3a. The PL spectrum of P3HT comprises several vibronic bands and peaks at 1.75 eV. Addition of 60% w/w of D99'BF to P3HT quenched the PL emission by a factor of approximately 100. As established in the early studies in the field, the near-total quenching of the PL results from photoinduced charge transfer and charge separation.^[12–15]

Figure 3b shows the PC obtained from thin films of pristine P3HT and the composite of P3HT:D99'BF. The energy gap inferred from the steady state PC spectral profiles of both the pristine P3HT and the BHJ films (655 nm; see Figure 3b) are nearly identical to the E_{G} obtained from absorption spectra (Figure 1b). The difference in photoresponsivity is, however, remarkable. The PC is strongly sensitized in the P3HT:D99'BF BHJ composites; an increase of more than 20 times is obtained after addition of D99'BF to P3HT. The PC of P3HT:D99'BF composites is more than 3 orders of magnitude larger than that obtained from pristine D99'BF. These data are in good agreement with results obtained from typical polymer/fullerene BHJ materials where electron transfer from the semiconducting polymer donor to the fullerene acceptor quenches the PL with a corresponding increase in the yield of photogenerated mobile charge carriers.^[12–15]

Figure 4a compares the dynamics of the time resolved PIA in thin films of pristine P3HT and P3HT:D99'BF probed at 4.8 μm and pumped at 400 nm where both P3HT and D99'BF have strong absorption. In this mid-IR spectral region, where the well-known polaron signatures of P3HT are detected,^[12–15] relatively fast decay was observed in P3HT. The much longer polaron lifetime in P3HT:D99'BF compared to that in the pristine polymer indicates the photogeneration of long-lived

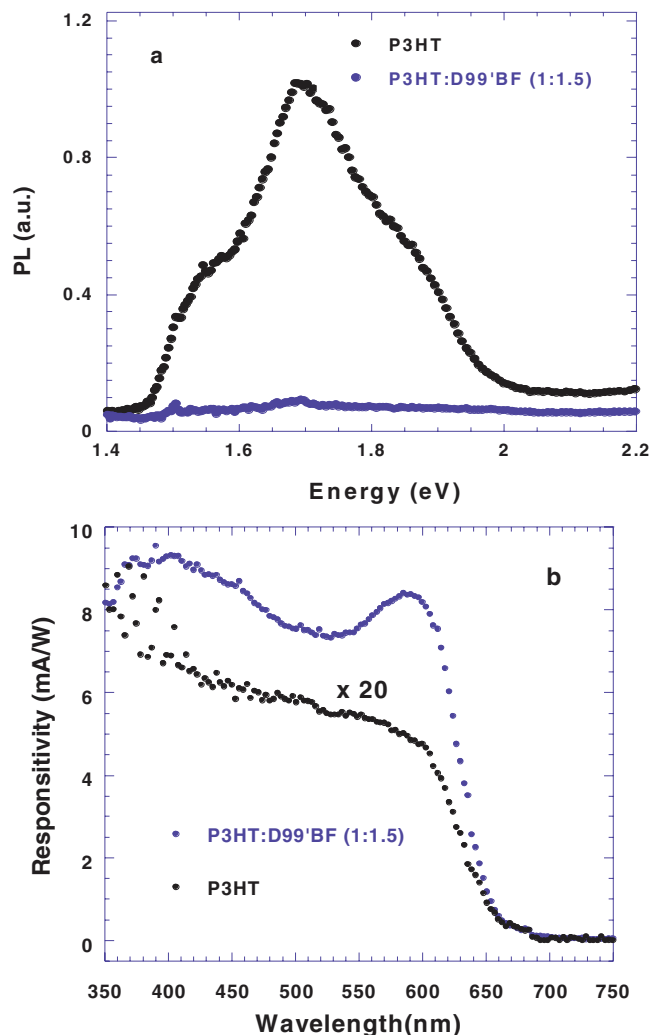


Figure 3. (a) Photoluminescence spectra of pristine P3HT, D99'BF and P3HT:D99'BF; (b) Comparison of the steady state photoconductivities (PC) of pristine P3HT, and P3HT:D99'BF. Note: the PC obtained from pristine D99'BF (not shown) is 3 orders of magnitude smaller than that of P3HT:D99'BF.

carriers, consistent with efficient electron transfer from P3HT to D99'BF and hole transfer from D99'BF to P3HT, and with inhibited back-transfer.^[15]

As noted above, hole transfer from D99'BF to P3HT is expected from the measured HOMO-HOMO offset. In order to specifically confirm efficient electron transfer from P3HT to D99'BF, we have investigated the time resolved PIA in pristine P3HT and P3HT:D99'BF following photo-excitation at 625 nm where P3HT has strong absorption, but D99'BF has negligible absorption (Figure 1b). The dynamics of the time resolved PIA in pristine P3HT and P3HT:D99'BF are shown in Figure 4b. Ultrafast photo-generation and P3HT polarons with long lifetime are observed on the P3HT component of P3HT:D99'BF following excitation at 625 nm. Note that at 625 nm, the photoresponsivity of P3HT:D99'BF is still a factor of 40 larger than the photoresponsivity of pristine P3HT. Thus mobile polarons are created on the P3HT chains by pumping at 625 nm. The

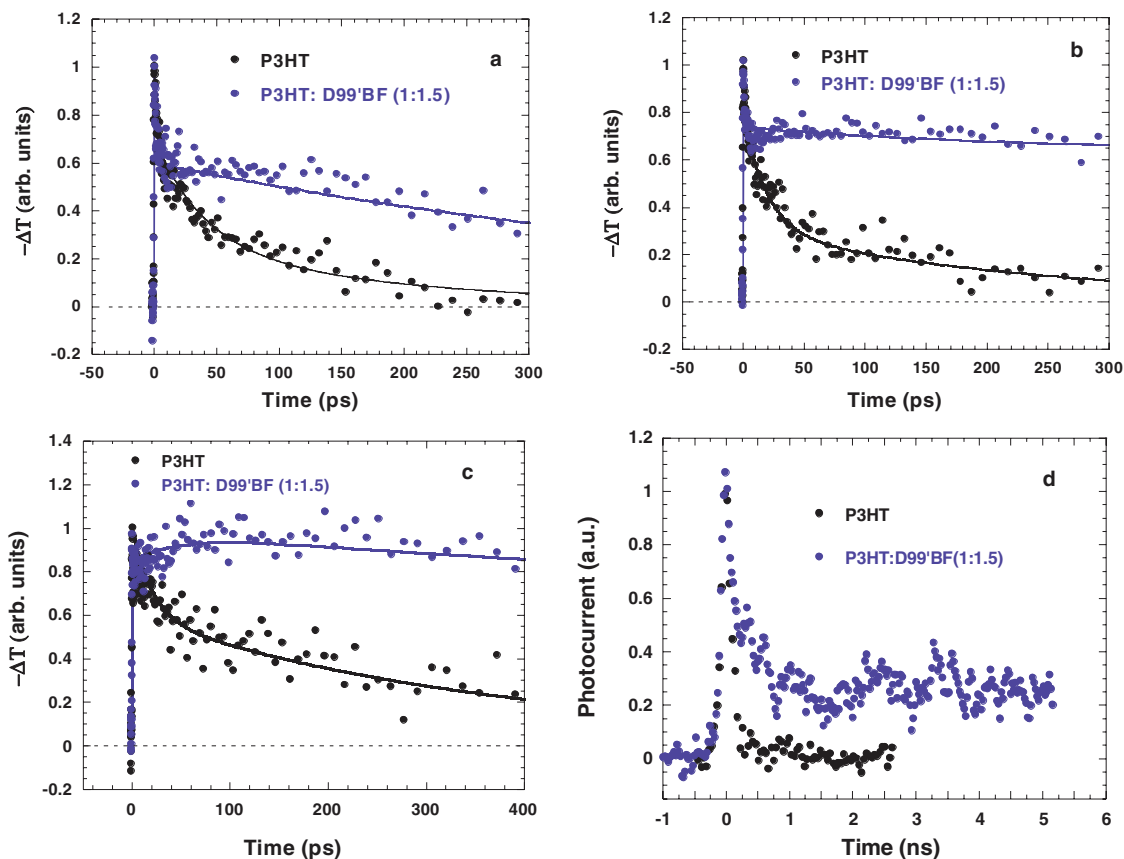


Figure 4. Mid-IR transient decay dynamics of P3HT and P3HT:D99'BF probed at 4.8 μm , pumped (a) at 400 nm, (b) at 625 nm and (c) 660 nm; (d) transient photocurrent at longer times following photoexcitation.

data in Figure 4b demonstrate efficient photo-induced electron transfer from P3HT to D99'BF even with only 0.12 eV difference between the LUMO energy of P3HT and the LUMO energy of D99'BF (Figure 1c).

After excitation at 660 nm (even deeper in the absorption tail; see Figure 1b), the polaron lifetime is significantly longer, but the photoresponsivity is essentially indistinguishable from that of P3HT (see Figure 4c). Thus the PIA detected at 4.8 μm following pumping at 660nm implies the formation of bound and immobile polarons. The crossover from photogeneration of mobile polarons to photogeneration of bound and immobile polarons occurs at precisely the energy predicted by the independently measured LUMO offset; the crossover occurs approximately 0.1 eV below the band edge (see Figures 1b and 3b). This bound polaron generated by pumping deep in the absorption tail could be either a component of an interfacial exciton or a polaron caught in an interfacial trap^[16–18] formed at the interface between P3HT and D99'BF. Transient photoconductivity measurements on operating P3HT:PCBM solar cells have shown that geminate recombination from interfacial excitons is small compared to recombination via interfacial traps.^[19,20] Thus, the PIA generated at 4.8 μm by pumping at 660 nm probably arises from polarons bound in interfacial traps.

The mobile carrier decay (photocurrent) at longer times was studied using transient photoconductivity measurements. Figure 4d shows the normalized transient photocurrent

waveforms obtained from thin films of P3HT and P3HT:D99'BF. Whereas the charge carrier decay in pristine P3HT is very fast (less than approx. 200 ps), the photocurrent response in P3HT:D99'BF shows a long lived component with essentially constant magnitude out to times beyond 5 ns. Thus, in P3HT:D99'BF, the photo-generated mobile charge carriers exhibit the long lifetime required for collection at the electrodes in BHJ solar cells. The ultrafast charge separation and long mobile carrier lifetime result in the high photocurrent observed in P3HT:D99'BF composites (see Figure 5a).

In order to evaluate the expected increase in V_{oc} , BHJ solar cells were fabricated with P3HT:D99'BF. The charge separating layer was a P3HT:D99'BF blend with 1:1.5 weight ratio. The current-voltage curves of BHJ PSCs with aluminum (Al), barium (Ba) and t-Bu-PBD-SO₃Na/Al as the cathodes are shown in Figure 5a. With Al as the cathode, P3HT:D99'BF PSCs yield a short-circuit current density (J_{sc}) $J_{\text{sc}} = 1.99 \text{ mA/cm}^2$, $V_{\text{oc}} = 0.58 \text{ V}$, a fill factor (FF), $\text{FF} = 0.32$, and $\text{PCE} = 0.36\%$. With the same active layer, the BHJ PSCs with Ba as the cathode yield the following: $J_{\text{sc}} = 3.9 \text{ mA/cm}^2$, $V_{\text{oc}} = 1.10 \text{ V}$, $\text{FF} = 0.40$, $\text{PCE} = 1.70\%$

Note that a larger V_{oc} (1.10 V) and a factor of 5 increase in PCE were observed from the PSCs with Ba as the cathode (rather than Al). With Ca as the cathode, $V_{\text{oc}} = 1.04 \text{ V}$. With t-Bu-PBD-SO₃Na/Al^[21] as the cathode, $V_{\text{oc}} = 1.20 \text{ V}$; approximately twice that obtained from P3HT:PCBM PSCs.

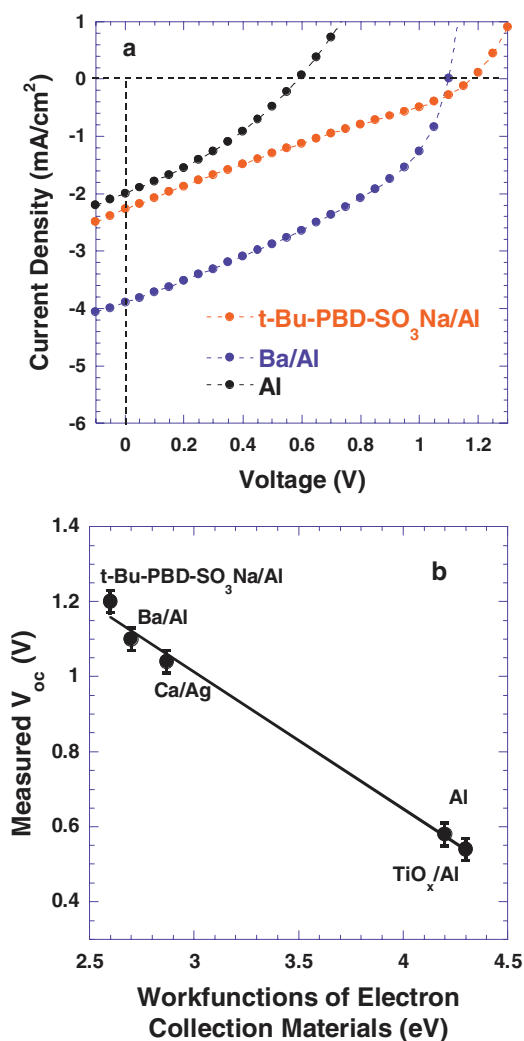


Figure 5. (a) J - V characteristics of semiconducting polymer solar cells under AM1.5G illumination from a calibrated solar simulator with an intensity of 100 mW/cm^2 with Al, Ba and *t*-Bu-PBD-SO₃Na/Al as cathode materials (see text), and (b) measured open circuit voltage (V_{oc}) versus the workfunction of the electron collection materials for semiconducting polymer solar cells with P3HT:D99'BF as the BHJ Layer.

In order to understand why the P3HT:D99'BF PSCs have low J_{sc} , we have measured the electron transport mobility of D99'BF using the transconductance of organic field-effect transistors (OFETs). D99'BF shows typical characteristics expected for n-type OFETs, but the electron mobility is approximately $10^{-5} \text{ cm}^2/\text{V}\cdot\text{s}$, more than two orders magnitude smaller than the hole mobility observed from P3HT.^[22,23] Therefore, the low J_{sc} from P3HT:D99'BF BHJ PSCs results at least in part from the low mobility of D99'BF. The low fill factors and modest efficiencies also imply relatively poor electron transport through the D99'BF nanostructure (poor connectivity). This morphology issue will have to be addressed in order to take full benefit in the increased open circuit voltage.

In Figure 5b, the measured V_{oc} data are plotted versus the workfunction of the electron collection materials. When the

work function of the cathode (-4.26 eV for Al, -4.30 eV for TiO_x/Al^[24]) is lower than the LUMO energy level of D99'BF (-3.1 eV), the Fermi energy is pinned at the electrode value, and energy is lost in the transfer of electrons from the D99'BF to the cathode. Specifically, for example, the TiO_x layer breaks the symmetry in the ITO/PEDOT/P3HT:D99'BF/TiO_x/Al cell, and the Fermi Level is pinned at the LUMO energy of TiO_x. Therefore, for Al and TiO_x/Al as cathodes, $V_{oc} \approx 0.58 \text{ V}$ and $V_{oc} \approx 0.54 \text{ V}$, respectively, consistent with the energy level diagrams in Figure 1c.

Higher V_{oc} values are obtained with lower work function cathodes. With Ba as the cathode, $V_{oc} = 1.10 \text{ V}$, and with Ca as the cathode, $V_{oc} = 1.04 \text{ V}$. When the work function of the cathode is closer to the vacuum level than the LUMO energy level of D99'BF (-3.12 eV), alignment of the Fermi level is achieved by charge transfer of electrons from the cathode into the D99'BF, and an ohmic contact is formed. As a result, the Fermi energy is pinned close to the LUMO level of D99'BF.^[25-27] The increase in V_{oc} with Ba relative to Ca is consistent with the different work functions (-2.70 eV for Ba; and -2.87 eV for Ca).^[28] With ITO/PEDOT/P3HT:D99'BF/*t*-Bu-PBD-SO₃Na/Al, $V_{oc} = 1.20 \text{ V}$. All these results demonstrate that V_{oc} values close to the band gap of the semiconducting polymer should be possible for BHJ solar cells just as for inorganic solar cells.

In conclusion, we have characterized the new electron acceptor D99'BF and the P3HT:D99'BF BHJ material. D99'BF exhibits strong optical absorption over the spectral range from 4 eV to 1.9 eV . When blended with P3HT, it increases the optical density and improves the light harvesting in this spectral range. Ultrafast charge transfer and charge separation are demonstrated in P3HT:D99'BF BHJ films. Photoinduced electron transfer from P3HT to the D99'BF yields mobile carriers with long lifetimes.

We have demonstrated that electron transfer occurs even though $E_{LUMO}(\text{P3HT}) - E_{LUMO}(\text{D99'BF}) \approx 0.12 \text{ eV}$. Thus, large LUMO band offsets are not required for charge separation. The exciton binding energy in P3HT must be less than approximately 0.1 eV .

BHJ PSCs fabricated using P3HT:D99'BF phase separated composites exhibit an open circuit voltage, $V_{oc} = 1.20 \text{ V}$ (under AM1.5 solar radiation), close to the theoretical maximum estimated from the difference in the energy levels of the HOMO of P3HT and LUMO of D99'BF, indicating that V_{oc} values close to the band gap of the semiconducting polymer should be possible for BHJ PSCs just as for inorganic solar cells.

Experimental Section

Absorption and Photoluminescence Spectra: For spectroscopic measurements, thin films were prepared by spin-casting from a 1 wt% dichlorobenzene solution, comprising either pure P3HT, pure D99'BF or P3HT:D99'BF at 1:1.5 weight ratio onto quartz substrates, resulting in a film thickness of $\sim 100 \text{ nm}$. The absorption spectra were measured with a Shimadzu UV-2401PC UV-visible spectrophotometer. Photoluminescence spectra were collected on a PSI (Photon Technology International) fluorescence system at room temperature.

Ultraviolet Photoelectron Spectroscopy (UPS): For UPS measurements, a 100 nm thick Au film was deposited on pre-cleaned Si substrates with a thin native oxide. P3HT solution in dichlorobenzene, 0.2% (w/v), was spin cast at spin speeds of 2000 rpm for 60 sec. D99'BF solution in dichlorobenzene 0.3% (w/v), was spin cast at spin speeds of 3000 rpm

for 60 sec. All films were fabricated inside a N₂ atmosphere glovebox and were transferred via an airtight sample holder to the UPS analysis chamber. Samples were also kept in a high vacuum chamber overnight to remove solvent residues. The UPS analysis chamber was equipped with a hemispherical electron energy analyzer (Kratos Ultra Spectrometer) and was maintained at 1×10^{-9} Torr. The UPS measurements were carried out using the He I ($h\nu = 21.2$ eV) source. During UPS measurements, a sample bias of -9 V was used in order to separate the sample and the secondary edge for the analyzer.

Photoconductivity and Time Resolved Photoinduced Absorption: Films used for the photoconductivity measurement were spin-cast onto alumina substrates from a 1 wt% dichlorobenzene solution, comprising pure P3HT, D99'BF or P3HT:D99'BF at 1:1.5 weight ratio, resulting in a film thickness of ~ 100 nm. The Auston switch sample geometry was used, with gold contacts $50 \mu\text{m}$ apart evaporated onto the thin films. Photocurrent transients were generated by pulsed-laser photoexcitation under an applied electric field ($F \sim 1 \times 10^4$ Vcm⁻¹). The photocurrent waveforms were recorded by a Boxcar integrator (EG&G PAR 4400). The laser pulses (100 fs duration, 1 KHz repetition rate) were produced by a Ti:sapphire system (Spectra Physics), where an optical parametric amplifier (OPA) was used to tune the excitation wavelength to values near the semiconducting polymer absorption maximum (570 nm for P3HT). The laser pulse intensity was $I \sim 1 \times 10^{-4}$ J cm⁻². Steady-state photoconductivity measurements were carried out by the conventional modulation technique and recorded by a lock-in amplifier; the light source was a xenon lamp and the light was modulated at 166 Hz. The applied electric field was $F = 1.5 \times 10^4$ Vcm⁻¹. The data were normalized by the measuring system response obtained after each run with a calibrated Si photodiode. All measurements were performed in vacuum ($P < 10^{-4}$ Torr). Films used for the time resolved photoinduced absorption measurement were spin-cast onto sapphire substrates from a 1 wt% dichlorobenzene solution, either pure P3HT or P3HT:D99'BF at 1:1.5 weight ratio, resulting in a film thickness of ~ 100 nm. The details of experimental set-up and the measurements are described in earlier publications.

Bulk Heterojunction Solar Cells: Solar cells were fabricated using P3HT as the electron donor and the D99'BF as the acceptor. The ITO-coated glass substrates were cleaned with detergent, distilled water, acetone, and isopropyl alcohol in an ultrasonic bath and then dried overnight in an oven at >100 °C. After treatment of the ITO substrates with UV ozone for 40 min, highly conducting PEDOT:PSS was spin-cast from aqueous solution (5000 rpm, thickness of ~ 40 nm). The substrates were dried at 160 °C for 10 min in air and transferred to a nitrogen-filled glovebox for spin-casting the P3HT:D99'BF layer. The dichlorobenzene solution, comprising P3HT:D99'BF at 1:1.5 weight ratio, was spin-cast on top of the PEDOT:PSS layer. The thickness of the active layer was ~ 100 nm. Subsequently, a thin layer of cathode, Ba (5nm) coated with Al (150 nm), Ca (10 nm) coated with Ag (150 nm) or Al (150 nm) was thermally deposited on BHJ layer through a shadow mask under vacuum. For solar cells with either t-Bu-PBD-SO₃Na or TiO_x as buffer layer, a thin layer (<20 nm) was spin-cast on top of active layer from t-Bu-PBD-SO₃Na in methanol solution or TiO_x in methanol solution, followed by thermal annealing at approximately 90 °C. Subsequently, a thin layer cathode, Al (150 nm) was thermally deposited on the buffer layer through a shadow mask under vacuum. The area of the cathode that defines the active area of the device was 4.5 mm². All data were obtained under white light AM1.5G illumination from a calibrated solar simulator with irradiation intensity of 100 mW/cm².

Acknowledgements

This research was supported by a grant from Konarka Technologies, Inc. and by support from the US Army General Technical Services (LLC/

GTS-S-09-1-196) and by the Department of Energy (BES-DOE- ER46535). FW and FB thank the MRL for support through a seed grant.

Received: October 12, 2010

Published online:

- [1] S. H. Park, A. Roy, S. Beaupré, S. Cho, N. Coates, J. S. Moon, D. Moses, M. Leclerc, K. Lee, A. J. Heeger, *Nat. Photon.* **2009**, *3*, 297.
- [2] Y. Liang, Z. Xu, J. Xia, S.-T. Tsai, Y. Wu, G. Li, C. Ray, L. Yu, *Adv. Mater.* **2010**, *22*, E135.
- [3] M. C. Scharber, D. Mühlbacher, M. Koppe, P. Denk, C. Waldauf, A. J. Heeger, C. J. Brabec, *Adv. Mater.* **2006**, *18*, 789.
- [4] G. Dennler, M. C. Scharber, T. Ameri, P. Denk, K. Forberich, C. Waldauf, C. J. Brabec, *Adv. Mater.* **2008**, *20*, 579.
- [5] N. Blouin, A. Michaud, D. Gendron, S. Wakim, E. Blair, R. Neagu-Plesu, M. Belletête, G. Durocher, Y. Tao, M. Leclerc, *J. Am. Chem. Soc.* **2008**, *130*, 732.
- [6] R. B. Ross, C. M. Cardona, D. M. Guldi, S. G. Sankaranarayanan, M. O. Reese, N. Kopidakis, J. Peet, B. Walker, G. C. Bazan, E. V. Keuren, B. C. Holloway, M. Drees, *Nature Mater.* **2009**, *8*, 208.
- [7] D. F. Kronholm, J. C. Hummelen, *Org. Photovoltaics* **2008**, 155.
- [8] J. H. Seo, T.-Q. Nguyen, *J. Am. Chem. Soc.* **2008**, *130*, 10042.
- [9] W. R. Salaneck, M. Lögdlund, M. Fahlman, G. Greczynski, T. Kugler, *Mater. Sci. Eng.* **2001**, *R34*, 121.
- [10] J. L. Brédas, D. Beljonne, V. Coropceanu, J. Cornil, *Chem. Rev.* **2004**, *104*, 4971.
- [11] H. Hoppe, N. S. Sariciftci, *Adv. Polym. Sci.* **2008**, 214, 1.
- [12] N. S. Sariciftci, L. Smilowitz, A. J. Heeger, F. Wudl, *Science* **1992**, *258*, 1474.
- [13] C. H. Lee, G. Yu, D. Moses, K. Padbaz, C. Zang, N. S. Sariciftci, A. J. Heeger, F. Wudl, *Phys. Rev. B* **1993**, *48*, 15425.
- [14] L. Smilowitz, N. S. Sariciftci, R. Wu, C. Gettinger, A. J. Heeger, F. Wudl, *Phys. Rev. B* **1993**, *47*, 13835.
- [15] C. X. Sheng, M. Tong, S. Singh, Z. V. Vardeny, *Phys. Rev. B* **2007**, *75*, 085206.
- [16] M. H. Tong, N. E. Coates, D. Moses, A. J. Heeger, *Phys. Rev. B* **2010**, *81*, 125210.
- [17] K. Vandewal, K. Tvingstedt, A. Gadisa, O. Inganäs, J. V. Manca, *Phys. Rev. B* **2010**, *81*, 125204.
- [18] I. W. Hwang, J. Kim, S. Cho, J. Yuen, N. Coates, K. Lee, M. Heeney, I. McCulloch, D. Moses, A. J. Heeger, *J. Phys. Chem. C* **2008**, *112*, 7853.
- [19] R. A. Street, M. Schoendorf, A. Roy, J. H. Lee, *Phys. Rev. B* **2010**, *81*, 205307.
- [20] R. A. Street, S. Cowan, A. J. Heeger, *Phys. Rev.*, **2010**, *82*, 121301.
- [21] X. Gong, S. Wang, D. Moses, G. C. Bazan, A. J. Heeger, *Adv. Mater.* **2005**, *17*, 2053.
- [22] S. Cho, J. Yuen, J. Kim, K. Lee, A. J. Heeger, *Appl. Phys. Lett.* **2006**, *89*, 153505.
- [23] M. Morana, P. Koers, C. Waldauf, M. Koppe, D. Muehlbacher, P. Denk, M. Scharber, D. Waller, C. Brabec, *Adv. Func. Mater.* **2007**, *17*, 3274.
- [24] J. Y. Kim, S. H. Kim, H.-H. Lee, K. Lee, W. Ma, X. Gong, A. J. Heeger, *Adv. Mater.* **2006**, *18*, 572.
- [25] S. M. Sze, K. K. Ng, *Physics of semiconductor devices*, 3rd Ed., A John Wiley & Sons, Inc. **2007**, P79–197.
- [26] R. I. Frank, J. G. Simmons, *J. Appl. Phys.* **1967**, *38*, 832.
- [27] G. G. Malliaras, *J. Appl. Phys.* **1998**, *84*, 1583.